

## RESEARCH ARTICLE

# A Hierarchical Control of Supercapacitor and Microsources in Islanded DC Microgrids

FARHAD BARATI<sup>1</sup>, BEHZAD AHMADI<sup>2</sup>, AND OZAN KEYSAN<sup>3</sup>

<sup>1</sup>Department of Energy, Materials and Energy Research Center, Karaj, Iran

<sup>2</sup>D&V Electronics, Woodbridge, ON L4H 2Y7, Canada

<sup>3</sup>Center for Solar Energy Research and Applications (ODTÜ-GÜNAM), Middle East Technical University, 06800 Ankara, Turkey

Corresponding author: Farhad Barati (f.barati@merc.ac.ir)

**ABSTRACT** This paper proposes a hierarchical control approach for SuperCapacitor (SC) energy storage and microsources in islanded DC microgrids. It takes into account microsources' dynamic and steady-state limitations. The proposed approach relies on an architecture presented for the SC's and microsources' interfaces with the DC bus. In the proposed architecture, DC microsources interface with the DC bus through buck converters. Moreover, the SC interfaces with the DC bus through the bi-directional buck converter. The instantaneous loads currents are measured and employed in the secondary control to calculate the reference currents for buck converters. In the primary control, we run buck converters as current sources. Moreover, the bi-directional buck converter is run to regulate the DC bus voltage. The proposed approach is generic; meaning that it can be employed for any islanded DC microgrid. Without loss of generality, to prove its effectiveness, we utilized it for a Low Voltage DC (LVDC) microgrid in this paper. Analysis, design, simulations, and experimental verifications are presented for the LVDC microgrid. The experimental results confirm that, by employing the proposed approach, the DC bus voltage deviations from its reference voltage is 5% and it restores in less than 1 sec.

**INDEX TERMS** Islanded DC microgrids, hierarchical control, SC energy storage, microsources' dynamic and steady-state limitations.

## I. INTRODUCTION

Nowadays, microgrids are known as effective solutions for integrating Distributed Energy Resources (DER) with Energy Storage Devices (ESD) and loads. They are classified as AC or DC, renewable-based or non-renewable-based, and grid-interactive or islanded ones [1], [2]. DC microgrids have several advantages over AC microgrids. In fact, in DC microgrids, fewer power conversion stages are required. Also, in DC microgrids, reactive power problem and synchronization problem do not exist [3], [4], [5]. On the other hand, fault current management in DC microgrids is a challenging issue while the fault current is well managed in AC microgrids. This is due to the fact that, an AC fault current can be cleared easily whenever it reaches zero. A DC fault current, however, never reaches zero [6].

The associate editor coordinating the review of this manuscript and approving it for publication was Guijun Li<sup>1</sup>.

TABLE 1. Nomenclature.

Symbol	Description
$C_{bus}$	DC bus capacitor
$V_{bus}, V_{Ref}$	DC bus voltage actual and reference values
$i_s, i_l$	Source and load converters' currents
$i_{es}$	Current absorbed from or injected to DC bus from SC's converter
$V_{sc}, i_{sc}$	SC's voltage and current
$i_{\Delta}$	Disturbance current
$i_{s,rf}$	Source converter's reference current
$\omega_n, \zeta$	Natural frequency and damping ratio

Renewable energy sources and Electric or Hybrid Electric Vehicles (HEV) have been the main motivations for developing DC microgrids. By employing a DC microgrid, renewable energy sources such as Photovoltaics (PV) and

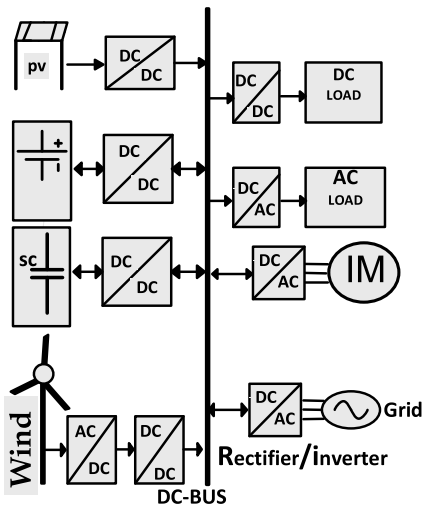


FIGURE 1. A grid-interactive renewable energy-based DC microgrid.

Wind are integrated with ESD and loads. The ESD may include batteries, SC, or a hybrid of them [7], [8].

A grid-interactive microgrid has the capability to inject power to the utility grid or absorb power from the utility grid if needed. However, an islanded microgrid, which has no interactions with the utility grid, needs to provide the load power demand by utilizing microsources and ESD [9], [10], [11], [12]. In such case, since microsources and ESD have limited capabilities and capacities, the provision of load power demand is always a challenging problem. In Fig.1, a grid-interactive renewable energy-based DC microgrid is shown. It is a generic architecture for a DC microgrid. If no rectifier/inverter is employed, an islanded microgrid is achieved. Also, if no PV and Wind exist, it can show the DC microgrid inside of an Electric or HEV. In the case of an Electric or HEV, the battery acts as the power source while the SC is the ESD. In addition to the propulsion motor, in an Electric or HEV, there are other AC and DC loads which are supplied through the DC bus.

An islanded DC microgrid must be equipped with an Energy Management System (EMS). Its role is to coordinate DER, ESD, and loads. More specifically, there are two main functions for an EMS. They include the DC bus voltage regulation and the load demand sharing between microsources. A hierarchical EMS is the most advanced and effective one. It includes the primary, secondary, and tertiary layers. The primary layer deals with the local control of power electronics converters based on the local measurements of voltages and currents. This layer is connected to the upper layers through the communication links. A reliable and high-bandwidth communication link guarantees a proper communication between different layers in a hierarchical EMS [13], [14].

Cascading control systems are presented for islanded DC microgrids with the purposes of DC bus voltage regulation and efficient load dispatch as in [15] and [16]. In [17], a power

management system is presented for a grid-interactive DC microgrid while in [18], for an islanded AC microgrid, renewable sources and battery energy storage are coordinately controlled. Two different secondary control are presented for islanded DC microgrids in [19] and [20]. They are non-droop-based and droop-based control systems as in [19] and [20], respectively. In [21], a dead-beat control is presented for islanded DC microgrids consisting of battery and SC energy storages. A reinforcement learning technique is presented to perform current sharing and voltage regulation in islanded DC microgrids as in [22].

None of the previous works have considered the limitations of microsources. In fact, any microsource, depending on its characteristics, has dynamic and steady-state limitations. These limitations must be considered in a microsource's operation in order to prevent excessive stresses on it. This guarantees the proper and safe operations of the microsource during its life time. The motivation of this work is to propose a high-performance control system for islanded DC microgrids in terms of both DC bus voltage regulation and load demand sharing while considering microsources' dynamic and steady-state limitations. The novel contributions of this paper are as follows.

- A hierarchical control approach consisting of secondary and primary control is presented. All of the instantaneous loads currents are measured and then transmitted to the secondary control using the communication link. The secondary control performs the load current sharing while considering dynamic and steady-state limitations of each of the microsources. The calculated reference currents are then transmitted to the primary layer using the communication link.
- An architecture is presented in which DC microsources and SC interface with the DC bus through buck and bi-directional buck converters, respectively. By using buck converters, we are able to control DC microsources as current sources. Moreover, the bi-directional buck converter gives us the opportunity to have a high-performance DC bus voltage control.

The idea of this work was first presented in [23] for an Electric Ship Medium-Voltage DC (MVDC) distribution system. It was proven using the numerical modeling and simulations in PSCAD/EMTDC software environment. The current paper is a generalized and comprehensively extended one compared to our previous work in [23] in terms of the followings.

- The idea is presented in a generic manner. So, it can be employed for islanded DC microgrids in any applications such as renewable energy systems, electric and hybrid electric vehicles, electric ships, and etc.
- The idea is implemented for a Low Voltage DC (LVDC) microgrid for which analysis, design, simulations, and experimental verifications are presented. The experimental results prove the idea in practice.

This paper is organized as follows. In section II, the proposed control approach is presented. The analysis, design,

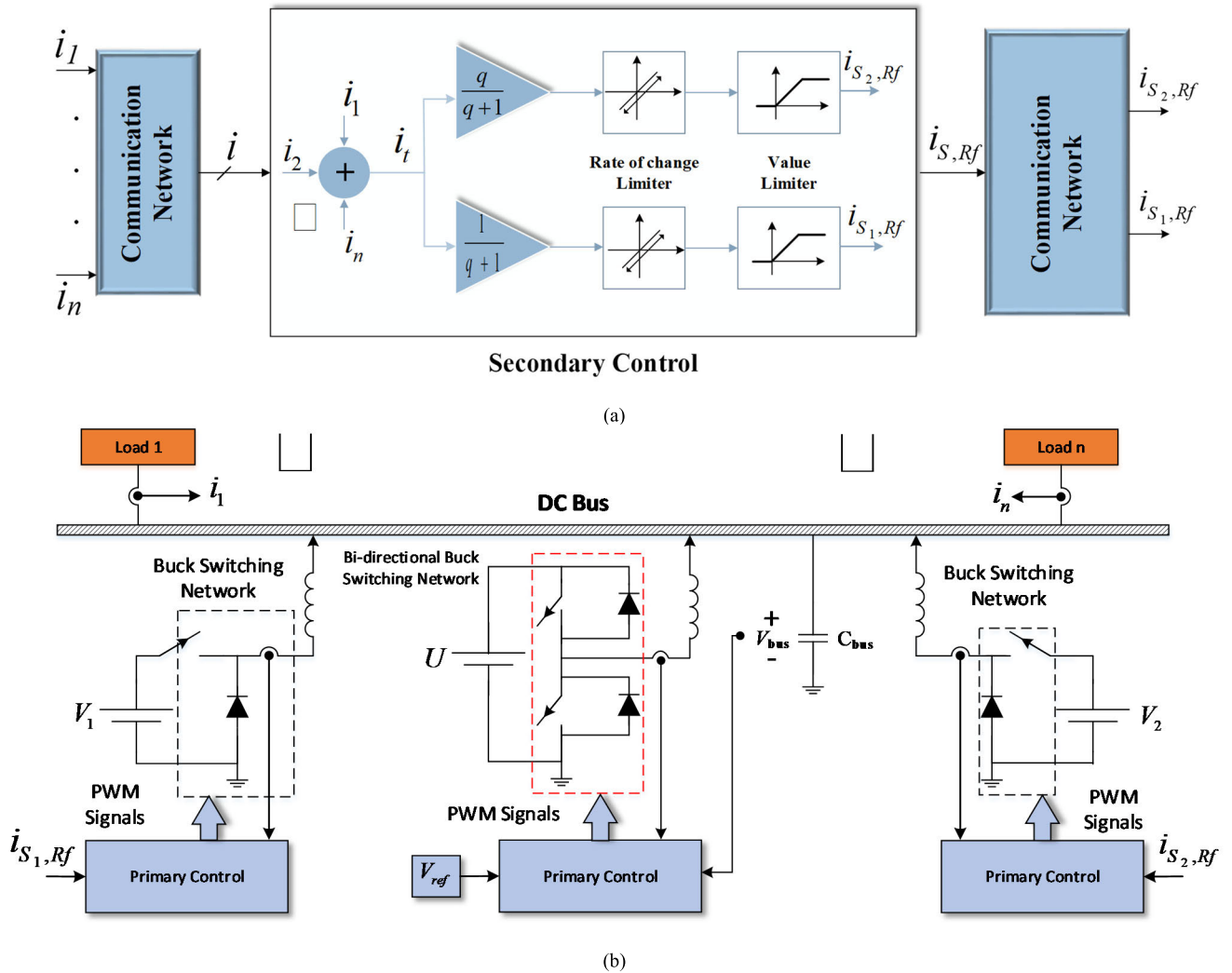


**FIGURE 2.** Proposed hierarchical control approach a) secondary control and communication network b) primary control and architecture for SC's and microsources' interfaces with DC bus.

and simulations of the primary control are presented in section III. In section IV, the experimental verification of the proposed approach is presented. Finally, in section V, the concluding remarks and future works are presented.

**II. PROPOSED HIERARCHICAL CONTROL APPROACH**

In Fig.2, the proposed hierarchical control approach is shown. As seen, it consists of secondary and primary control. The secondary control is linked to the microgrid through a communication network. The approach is generic; meaning that it can be employed for an islanded DC microgrid with any number of loads and sources.

**A. SECONDARY AND PRIMARY CONTROL**

In the proposed control approach, the instantaneous loads currents are measured. They are the currents absorbed by loads' converters from the DC bus. The measured currents are then transmitted to the secondary control through a

communication network. Since the measured currents may contain high frequency contents, a high-bandwidth communication network is needed.

In the secondary control, the total instantaneous load current is calculated as follows.

$$i_t = \sum_{k=1}^{k=n} i_k \tag{1}$$

We share the total instantaneous load current between microsources according to their power ratings. In Fig.2, without loss of generality, the approach is shown for two microsources. We assumed  $q$  as the ratio of source2's power rating to source1's power rating.

We know that any microsource has limitations in providing the power both at dynamic and steady-states. So, its limitations must be considered in its operation; otherwise it may fail or be damaged.

In the proposed approach, as seen, we considered two limiters. They are the rate of change limiter and the value

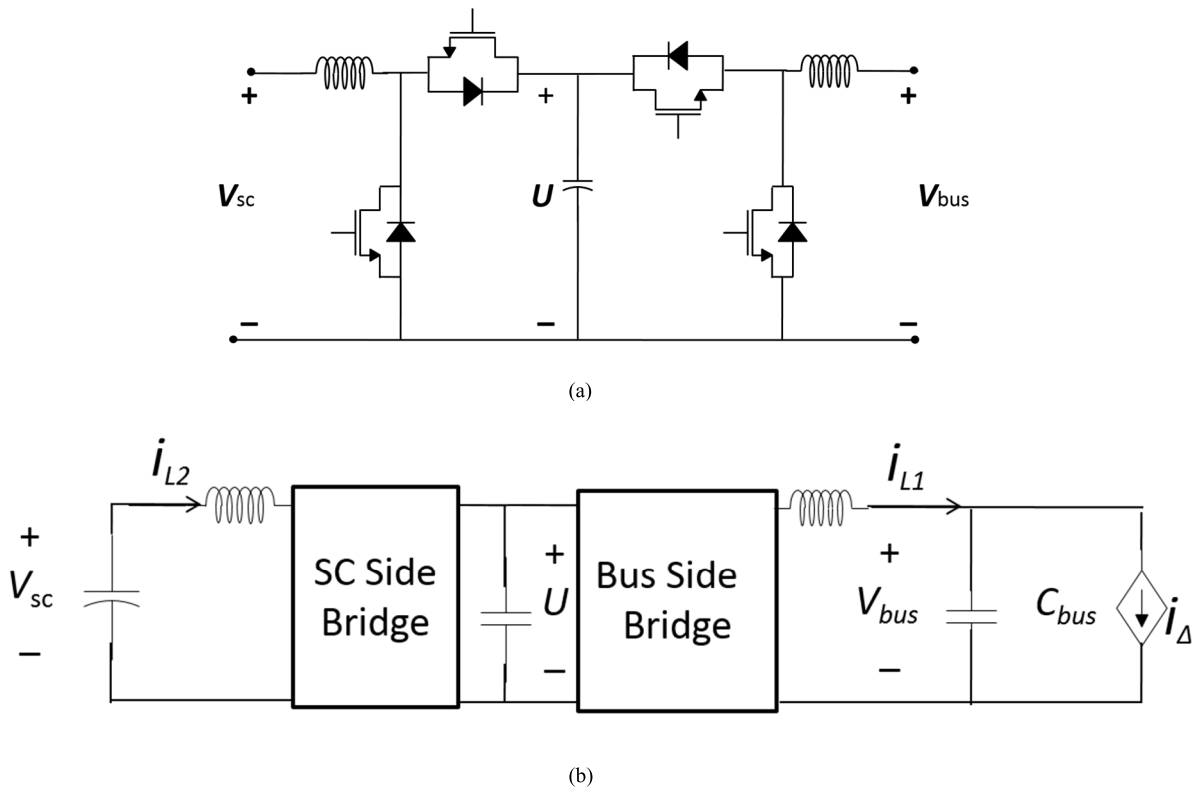


**FIGURE 3.** a) Bi-directional boost converter connected to SC along with bi-directional buck converter connected to DC bus b) an equivalent scheme for LVDC microgrid.

limiter. The rate of change limiter guarantees that no excessive stresses beyond the capabilities of the microsource are imposed at dynamic states. The value limiter, however, is implemented in order to avoid excessive stresses at steady-states. The reference currents are calculated in this way and then transmitted to the primary control through the communication network.

In the proposed approach, the primary control has two roles. The first role is to regulate the DC bus voltage at the reference voltage, i.e.  $V_{ref}$ . The reference voltage is constant and determined according to the power rating of the DC microgrid.

The second role is to make the currents injected from microsources' converters to the DC bus follow the reference currents, i.e.  $i_{S,Rf}$ .

**B. ARCHITECTURE FOR SC's AND MICROSOURCES' INTERFACES WITH DC BUS**

The proposed approach relies on an architecture for the SC's and microsources' interfaces with the DC bus. It is shown in Fig.(2-b). As seen, microsources interface with the DC bus through the buck converters. The letter  $V$  stands for a microsource's voltage or the output voltage of the converter connected to the microsource. The SC interfaces with the DC bus through the bi-directional buck converter as seen. The letter  $U$  stands for the SC's voltage or the output voltage of the converter connected to the SC. The DC bus is equipped

with a capacitor, i.e.  $C_{bus}$ , whose only role is to keep the DC bus voltage ripples within the acceptable range. This means that, in the proposed approach, the DC bus capacitor is not employed to compensate for mismatching between the demand and supplied powers. So, it can be chosen small.

Because of the limiters employed, the total current supplied by the buck converters, i.e.  $i_{st} = i_{s1,Rf} + i_{s2,Rf}$ , does not match the total load current, i.e.  $i_t$ . Therefore, the DC bus voltage tends to fluctuate. The bi-directional buck converter has to supply/absorb the difference between  $i_{st}$  and  $i_t$  in order to keep the DC bus voltage regulated. In fact, if  $i_{st}$  exceeds  $i_t$ , the DC bus voltage tends to swell which necessitates the absorption of difference by the bi-directional buck converter. The bi-directional buck converter, however, has to supply the difference between  $i_{st}$  and  $i_t$  if  $i_t$  exceeds  $i_{st}$ . By supplying or absorbing currents, the SC is discharged or charged, respectively.

In the following sections, without loss of generality, to prove its effectiveness, the proposed approach is implemented for an LVDC microgrid. Analysis, design, simulations, and experimental results are shown for the LVDC microgrid.

**III. PRIMARY CONTROL ANALYSIS AND DESIGN AND LVDC MICROGRID SIMULATIONS**

For an LVDC microgrid, in this section, analysis, design, and simulations of the primary control are presented. In the

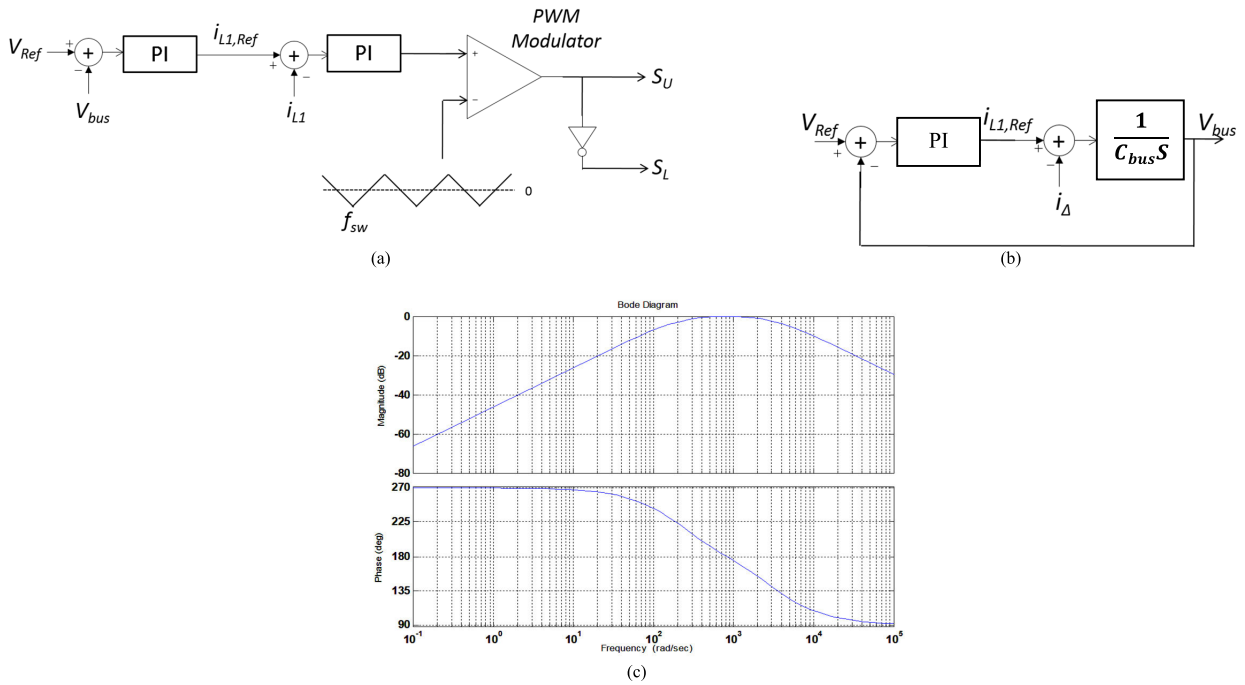


FIGURE 4. Designed closed-loop control system for DC bus voltage a) control structure b) equivalent block diagram c) Bode diagram.

LVDC microgrid, we considered a bi-directional boost converter as the converter connected to the SC. This converter is, of course, connected to the DC bus through the bi-directional buck converter as stated in section II. Each of the bi-directional boost or bi-directional buck converters consists of a Half-Bridge. We call the Half-Bridge of the bi-directional boost converter as the SC Side Bridge. Also, the Half-Bridge of the bi-directional buck converter is called as the Bus Side Bridge.

In Fig.(3-a), the bi-directional boost converter connected to the SC along with the bi-directional buck converter connected to the DC bus are shown. An equivalent scheme as shown in Fig.(3-a) is considered for the LVDC microgrid. In this scheme, the effects of loads and microsources are represented by  $i_{\Delta}$  which equals to  $i_{\Delta} = i_t - i_{st}$ . Moreover, the bi-directional boost converter is employed to regulate the intermediate bus voltage, i.e.  $U$ , as presented in [24] and [25].

### A. CONTROL OF BI-DIRECTIONAL BUCK CONVERTER

We design a high-bandwidth closed-loop control system for the DC bus voltage by employing the bi-directional buck converter. It is shown in Fig.(4-a). As seen, it includes the current closed-loop control as the inner loop whose role is to make the converter's output current follow the reference value, i.e.  $i_{L1,Ref}$ . A Proportional-Integral (PI) controller is employed for the current closed-loop control system. Moreover, a Pulse-Width Modulator (PWM) is utilized to generate switching signals for the power switches of the bi-directional buck converter. The symbols  $S_U$  and  $S_L$  denote switching signals for the upper switch and the lower switch in the Half-Bridge, respectively.

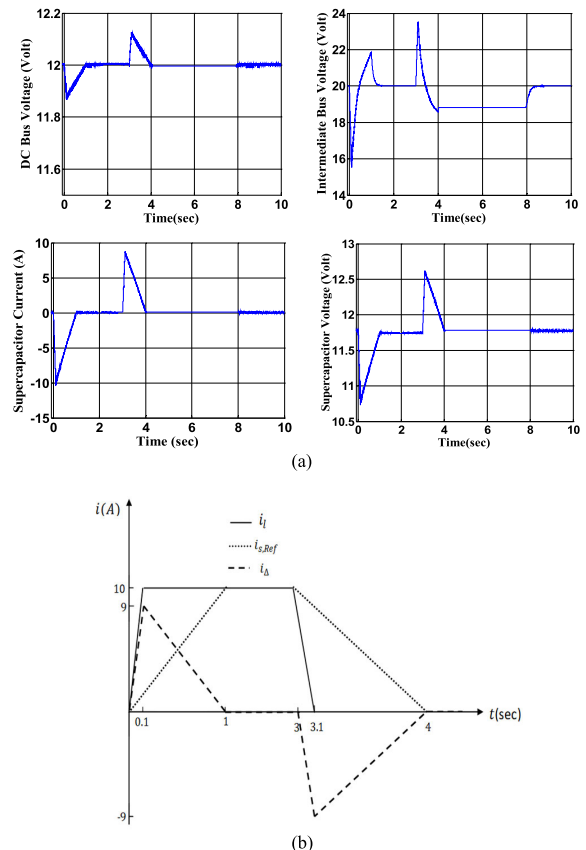


FIGURE 5. Simulations in PSCAD/EMTDC a) simulation results b) simulated load, source, and disturbance currents.

Suppose the current closed-loop control system is working properly; meaning that  $i_{L1,Ref} \approx i_{L1}$ . In this assumption, as

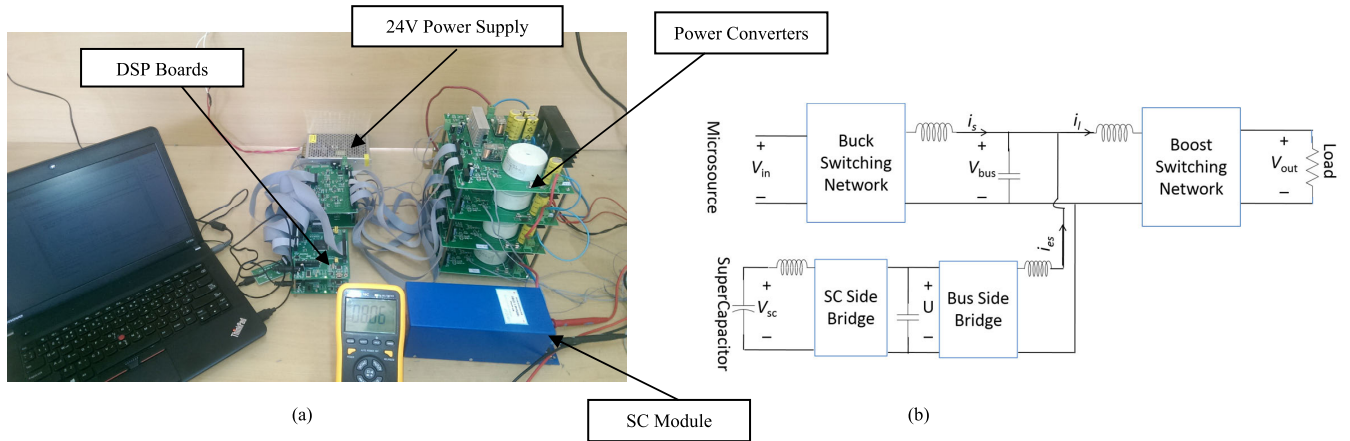


FIGURE 6. Experimental verifications a) set-up b) LVDC microgrid architecture.

usual, high frequency ripples in the converter’s output current are neglected. According to Fig.(3-b), one can write the DC bus voltage dynamics as follows.

$$i_{L1} - i_{\Delta} = C_{bus} \frac{dV_{bus}}{dt} \quad (2)$$

Based on the equation (2) and by considering  $i_{L1,Ref} \approx i_{L1}$ , an equivalent block diagram as in Fig.(4-b) can be derived. As clear,  $i_{\Delta}$  in this diagram behaves such as a disturbance which tends to introduce fluctuations in the DC bus voltage. According to Fig.(4-b), the transfer function from  $i_{\Delta}$  to the DC bus voltage is as the following.

$$\frac{V_{bus}(s)}{i_{\Delta}(s)} = -\frac{1}{K_i} \frac{\omega_n^2 s}{s^2 + 2\zeta\omega_n s + \omega_n^2} \quad (3)$$

where,  $\omega_n^2 = \frac{K_i}{C_{bus}}$  and  $\zeta = \frac{K_p}{2\sqrt{C_{bus}K_i}}$ .  $\omega_n$  is the natural frequency and  $\zeta$  is the damping ratio. Also,  $K_p$  and  $K_i$  are the voltage loop controller’s proportional and integral coefficients, respectively. As an example, it is clear from equation (3) that, a positive step in  $i_{\Delta}$  results in a transient sag at the DC bus voltage. The DC bus voltage is, however, restored to  $V_{ref}$  shortly.

For the designed controller parameters, as listed in Table 2, the Bode diagram of transfer function in (3) is depicted in Fig.(4-c). As clear, considerable attenuation is provided by the closed-loop control system at low frequencies. According to the proposed approach, it is expected that,  $i_{\Delta}$ , as the disturbance current, has its significant contents at low frequencies. So, we expect that the effects of  $i_{\Delta}$  on the DC bus voltage are compensated properly by the closed-loop control system.

### B. CONTROL OF BUCK CONVERTERS

The buck converters, as microsources’ interfaces with the DC bus in the proposed approach, are controlled as current sources. In the other words, the output current of each buck converter has to follow its reference current properly. For this purpose, we considered a control structure similar to the current closed-loop control system in Fig.(4-a). In the

control structure of each buck converter, the reference current is received from the secondary control, i.e.  $i_{S,Ref}$ . Also, a PI and a PWM are utilized as the controller and modulator, respectively. The controller’s coefficients are chosen such that, besides the closed-loop system stability, the converter’s output current follows the reference current properly [26].

### C. LVDC MICROGRID SIMULATIONS

We performed simulations in PSCAD/EMTDC software environment to evaluate the designed LVDC microgrid performance. For this purpose, we considered one load and one source. As defined before,  $i_{\Delta} = i_t - i_{st}$  where,  $i_t = \sum_{k=1}^{k=n} i_k$  and  $i_{st} = i_{S1,Ref} + i_{S2,Ref}$  for a DC microgrid with two sources. So,  $i_{\Delta} = i_t - i_{S,Ref}$  in the LVDC microgrid where,  $i_t$  is the current absorbed by the load converter from the DC bus. Also,  $i_{S,Ref}$  is the reference current for the source’s buck converter. We assume that the reference current is followed by the converter’s output current properly. So,  $i_s \approx i_{S,Ref}$  where,  $i_s$  is the current injected by the buck converter to the DC bus. In this assumption, high frequency ripples in the converter’s output current are neglected.

A simulated load current as shown in Fig.(5-b) is considered. According to the proposed approach, the load current is employed to calculate the reference current for the microsource’s buck converter. The reference current is calculated according to the limiters employed. In the simulations, we set the rate of change limits to  $\pm 10 A/sec$ . It means that in the calculated reference current, the rate of changes higher than  $+10 A/sec$  or lower than  $-10 A/sec$  does not exist. Also, we set the value limits to 10A and 0A. This means that the calculated reference current’s value is neither more than 10A nor less than 0A. We considered 10A as the nominal output current of the buck converter. Also, no negative current is allowed at the buck converter output.

We assume that the output current of buck converter follows the reference current properly. This results in an  $i_{\Delta}$  as shown in Fig.(5-b). According to Fig.(3-b), the  $i_{\Delta}$  introduces disturbances in the closed-loop control systems of the

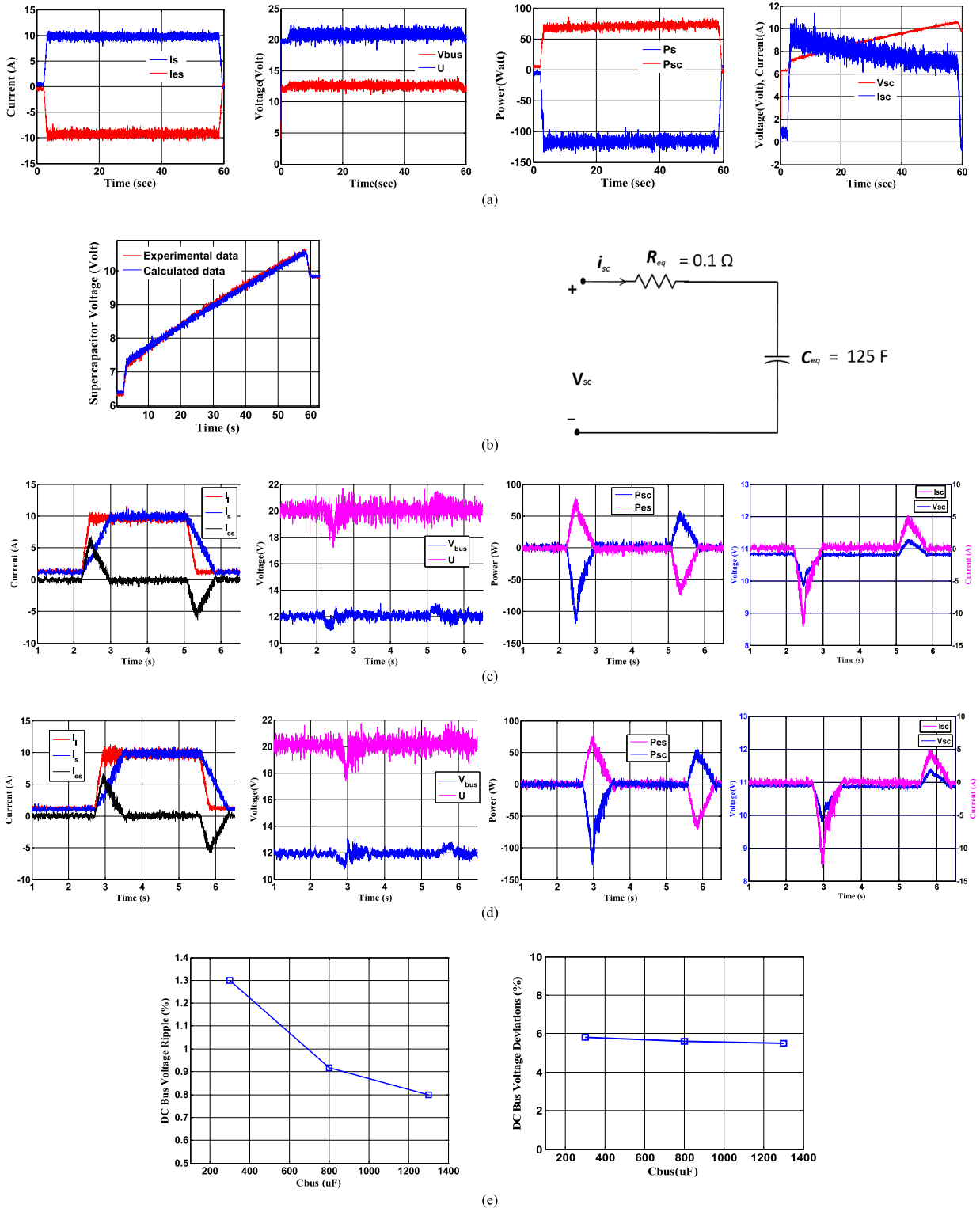


**FIGURE 7.** Experimental results a) SC initial charging procedure b) equivalent-circuit parameters for SC module c) verifications of proposed approach. d) test with 1mF capacitor added to DC bus e) quantitative comparison for different DC bus capacitors.

bi-directional buck and bi-directional boost converters. The results are shown in Fig.(5-a).

We set  $V_{ref} = 12V$  as the DC bus reference voltage. Also,  $U_{ref} = 20V$  is set as the intermediate bus reference voltage.

The SC's nominal voltage is 12V. It is almost fully charged at the beginnings of simulations. The DC bus voltage as well as the intermediate bus voltage are formed using the initial charging of the SC before the disturbance current is

**TABLE 2.** LVDC microgrid parameters.

Parameter	Value
SC Module	12V, 100F
DC bus Capacitor	$C_{bus} = 300\mu\text{F}$
Converters' Inductances	$L = 600\mu\text{H}$
Resistive Load	11 $\Omega$ , 500Watt
Power Source	60V, 300 Watt
Controller Boards	TMS320F28335 DSP Boards
DC Bus Reference Voltage	$V_{Ref} = 12\text{V}$
Intermediate Bus Reference Voltage	$U_{Ref} = 20\text{V}$
DC Bus Voltage Controller's Coefficients	$K_p=1, K_i=200$

introduced. As seen, the DC bus voltage experiences sag and swell whose amplitudes are less than 1%. The DC bus voltage is, however, restored as soon as the disturbance current vanishes. This proves the excellent performance of the designed closed-loop control system for the DC bus voltage.

The intermediate bus voltage, as seen, experiences fluctuations of less than 20% around its reference voltage, i.e. 20V, but it is quite stable. It is worth mentioning that, the DC bus voltage closed-loop control system behaves well as long as the intermediate bus voltage remains higher than the DC bus voltage. The SC charges/discharges according to the disturbance current. As clear, the SC discharges in order to prevent any voltage drop at the DC bus. Also, it charges in order to prevent any voltage swell at the DC bus. The SC's voltage varies according to its current as shown. In the SC's model in simulations, we considered an equivalent series resistance too whose effects, as seen, are sudden changes in the voltage as the current changes suddenly.

#### IV. EXPERIMENTAL VERIFICATIONS

An experimental set-up as shown in Fig.(6-a) is considered to verify the proposed control approach. It employs a 100F, 12V SC module with the bi-directional boost converter, as the converter connected to the SC, and the bi-directional buck converter as the SC's interface with the DC bus as seen in Fig.(6-b). In Fig.(6-b), the LVDC microgrid architecture is shown. As seen, in the LVDC microgrid, one microsource is considered whose converter is a buck one according to the proposed approach. Also, we considered one load which is connected to the DC bus through a boost converter. The experimental set-up parameters are listed in Table 2.

In Appendix, more details of the experimental set-up are presented.

##### A. INITIAL CHARGING PROCEDURE OF SC MODULE

In order to be able to exchange power, the SC needs to be charged to its nominal voltage at first. We do the initial charging of SC module using the experimental set-up

in which a 60V, 5A DC power supply is employed as the microsource. The experimental results are shown in Fig.(7-a). In this procedure, which no load is included, we run the buck converter to inject a 10A current to the DC bus. Since the bi-directional buck converter is responsible for the DC bus voltage control, it absorbs the injected current to the bus. The absorbed current tends to introduce a voltage swell at the intermediate bus which is compensated by the proper action of the bi-directional boost converter. In fact, the bi-directional boost converter absorbs the injected current to the intermediate bus in order to prevent a voltage swell which results in the SC charging. As can be seen, in this way, the SC is charged at an almost constant power; meaning that the charging current decreases as the SC's voltage rises. It is worth mentioning that, the intermediate as well as DC buses are, at the beginning, formed at their reference voltages. According to the power waveforms, one can calculate the efficiency from the DC bus to the SC in the charging mode. It equals to 62.5%. It is the multiplication of the efficiencies of the bi-directional buck and the bi-directional boost converters in the charging mode.

Based on the experimental data for the SC's voltage and current, we derive the equivalent-circuit parameters of the SC module. The equivalent-circuit considered is a simple, but an effective, one. In fact, it consists of a capacitor in series with a resistor. The derived equivalent-circuit parameters are  $R_{eq} = 0.1\Omega$  and  $C_{eq} = 125\text{F}$ . The simulation results of equivalent-circuit are compared with the experimental data in Fig.(7-b). As can be seen, a close agreement is achieved between the simulation and the experimental results. The equivalent-circuit parameters are employed in the previous section for the LVDC microgrid simulations.

##### B. VERIFICATIONS OF PROPOSED APPROACH

To verify the proposed approach, we considered a load current profile as shown in Fig.(7-c). In fact, the load converter, which is a boost one in the LVDC microgrid, is run to absorb the desired current profile from the DC bus. Since only one microsource is considered in the LVDC microgrid, no current sharing is required. According to the proposed approach, the instantaneous load current is employed to calculate the reference current for the microsource's buck converter. The calculation is performed based on the limits we considered for the rate of change and value limiters. We set  $\pm 11.76\text{A/sec}$  as the limits for the rate of change limiter. Also, 10A and 0A are considered as the limits of value limiter. The calculated reference current is properly followed by the buck converter's output current as shown in Fig.(7-c). Since the load current considered changes at higher rates, the rate of changes of buck converter's output current reaches the limits, i.e.  $\pm 11.76\text{A/sec}$ . Also, with the considered load current profile, the limits of value limiter are not exceeded.

The instantaneous difference between the load current and the buck converter's output current tends to introduce fluctuations in the DC bus voltage. Since the bi-directional buck converter is responsible for the DC bus voltage control, it has



to provide the difference. This action results in fluctuations in the intermediate bus voltage. Since the bi-directional boost converter attempts to keep the intermediate bus voltage regulated, its action results in charging or discharging of the SC. The SC charging or discharging current varies the SC's voltage accordingly.

As seen in Fig.(7-c), the DC bus voltage is regulated well. In fact, the DC bus voltage experiences fluctuations of less than 10% before restoring to its reference voltage, i.e. 12V. Also, the intermediate bus voltage experiences fluctuations of less than 15% before restoring to its reference voltage, i.e. 20V. As stated before, the bi-directional buck converter performs well as long as the intermediate bus voltage, i.e.  $U$ , is higher than the DC bus voltage.

### C. EFFECTS OF DC BUS CAPACITOR'S SIZE

In order to study the effects of DC bus capacitor's size in the proposed approach, a  $1mF$  capacitor is added to the DC bus and the previous test is repeated. The results are shown in Fig.(7-d). As can be seen, the results are very close to the previous test. The DC bus voltage is, however, different in terms of its ripples. In order to show the effects of DC bus capacitor's size on the DC bus voltage, a quantitative comparison is performed for three different values of capacitors, i.e.  $300\mu F$ ,  $800\mu F$ , and  $1300\mu F$  and the results are presented in Fig.(7-e). As seen, DC bus voltage ripples, as expected, are reduced by increasing in the DC bus capacitor's size. However, increasing in the DC bus capacitor's size does not significantly reduce the DC bus voltage deviations from the reference voltage as clear. This is due to the fact that, in the proposed control approach, the DC bus capacitor is not employed for mismatching compensations. Instead, a high-bandwidth DC bus voltage control system is employed. So, in the proposed approach, the DC bus capacitor's size, without degradations in the performance, can be reduced as long as DC bus voltage ripples are within the acceptable range. As seen in Table 2, we have chosen a  $300\mu F$  capacitor for the DC bus which results in the DC bus voltage ripples of about 1%.

A regenerative load may inject currents to the DC bus. An example of injecting currents to the DC bus from a regenerative load is the braking operation in an Electric or Hybrid Electric Vehicle. In such case, the reference current for the microsource's buck converter is set to zero. This is due to the fact that, a negative load current is blocked by the value limiter according to the proposed approach. Therefore, in order to keep the DC bus voltage regulated, the injected current from regenerative load is absorbed by the bi-directional buck converter. So, a similar scenario as shown in Fig.(7-a) occurs resulting in the absorption of regenerative energy by the SC.

Compared to the previous works, the proposed approach of this paper results in a much less DC bus voltage deviations from the reference voltage at a small DC bus capacitor. As seen in Fig.(7-e), the DC bus voltage deviation from the reference voltage is about 5% at the  $300\mu F$  DC bus capacitor. In [27], a DC bus capacitor equals to  $100\mu F$  is employed.

It resulted in the DC bus voltage deviation from the reference voltage equals to 23%. Although both of the  $100\mu F$  and  $300\mu F$  are small capacitors, the DC bus voltage deviation from the reference voltage is much less in the case of the proposed approach. Such achievement is at the result of the high-performance hierarchical control system employed.

### V. CONCLUDING REMARKS AND FUTURE WORKS

A hierarchical control system is proposed for islanded DC microgrids in this paper. It takes into account microsources' dynamic and steady-state limitations which guarantees their proper and safe operations during their life time. A well-regulated DC bus voltage is achieved by employing the proposed control approach at a small DC bus capacitor. So, the required DC bus capacitor is a low cost, volume, and weight one.

The DC bus capacitor feeds the DC bus fault. So, generally speaking, a small DC bus capacitor results in a low DC bus fault current. In this paper, the healthy operation of an islanded DC microgrid employing the proposed approach is considered. The faulty operation of an islanded DC microgrid employing the proposed approach, however, remains as the future works.

The communication links, depending on their bandwidth, may introduce time-delays. These delays exist both in calculating the reference currents based on the measured loads currents and in receiving the reference currents by the microsources' buck converters. At the result of communication links time-delays, the microsources' buck converters respond to loads currents changes with time-delays. Since the bi-directional buck converter has to regulate the DC bus voltage, in addition to transients, it has to supply the DC bus during time-delays too. This means that, besides the SC which supplies the required power during transients, we need to include the battery energy storage to supply the required energy during time-delays. So, as another future works, we consider the inclusion of battery energy storage in the proposed approach forming a Hybrid Energy Storage (HES).

### APPENDIX

In the experimental set-up, as shown in Fig.(6-a), a  $100F$ ,  $12V$  KAMCAP SC module is employed. The SC module utilizes a passive balancing approach in order to balance the voltage across the SC cells connected in series. In fact, in this module, two parallel branches each consisting of five series connected SC cells are employed. A nominal current of  $70A$  is considered for the SC module by the manufacturer.

In order to realize the power electronics converters exist in the LVDC microgrid, four similar Half-Bridge converters are employed. Each Half-Bridge converter is equipped with an inductor as well as input and output capacitors. We run the Half-Bridge converter associated with the microsource in the buck mode while the Half-Bridge converter associated with the load is run in the boost mode. The two other Half-Bridges are employed as the Bus Side and SC side Bridges as shown in Fig.(6-b). By connecting the Bus Side and SC Side Bridges in back-back, an intermediate bus capacitor equals to  $800\mu F$  is

achieved. This means that each of the Half-Bridge converters has an input capacitor equals to  $400\mu F$ . Also, the output capacitor of each of the Half-Bridge converters in the experimental set-up equal to  $100\mu F$ . Since the outputs of three Half-Bridge converters are connected to the DC bus as the source converter, load converter, and Bus Side Bridge, a DC bus capacitor equals to  $C_{bus} = 300\mu F$  is achieved.

A DC bus reference voltage equals to  $V_{Ref} = 12V$  and an intermediate bus reference voltage equals to  $U_{Ref} = 20V$  is considered in the LVDC microgrid. A switching frequency equals to  $f_{sw} = 20kHz$  is considered for each of the Half-Bridge converters. Also, an inductor equals to  $L = 600\mu H$  is considered for each of the Half-Bridge converters.

The inductors' currents are measured using Hall Effect Integrated Circuits (HEIC) that provide high-bandwidth current measurements. The HEIC employed are able to measure currents up to  $\pm 20A$  with high accuracy. As clear, an accurate current measurement is essential in the proposed control approach.

The Half-Bridges' input and output voltages are measured using two similar Opto-Coupler Integrated Circuits (IC). Both of the Hall Effect and Opto-Coupler ICs provide isolated grounds at their outputs. It makes having two separate grounds possible in experimental set-up.

The converters are controlled using two TMS320F28335 DSP boards. In fact, in the experimental set-up, the source and load converters are controlled using one of the DSPs while the Bus Side and SC Side Bridges are controlled using the other one. The converters are connected to the DSP boards using interface boards. In fact, the measured signals as well as PWM switching signals are subjected to noises which can deteriorate signals accuracy. In order to reduce noise effects in the experimental set-up, measured signals are amplified at the converters' boards but they are attenuated and filtered at the interface boards before connecting to the DSP boards. Also, PWM signals generated by the DSP boards are amplified which are then attenuated before connecting to the Power MOSFETs' Driver ICs. It is worth mentioning that each Half-Bridge converter is equipped with relays and fuses both at the input and output. The employment of relays gives us an extra protection opportunity which can be used to isolate the input or output in the case of a fault.

## ACKNOWLEDGMENT

The authors thank the University of Tabriz for the support of this work.

## REFERENCES

- [1] N. R. Tummuru, M. K. Mishra, and S. Srinivas, "Dynamic energy management of renewable grid integrated hybrid energy storage system," *IEEE Trans. Ind. Electron.*, vol. 62, no. 12, pp. 7728–7737, Dec. 2015.
- [2] K. S. El-Bidairia, H. D. Nguyen, S. D. G. Jayasinghe, T. S. Mahmoud, and I. Penesis, "A hybrid energy management and battery size optimization for standalone microgrids: A case study for Flinders island, Australia," *Energy Convers. Manage.*, vol. 175, pp. 192–212, Nov. 2018.
- [3] C. Sandoval, V. M. Alvarado, J.-C. Carmona, G. L. Lopez, and J. F. Gomez-Aguilar, "Energy management control strategy to improve the FC/SC dynamic behavior on hybrid electric vehicles: A frequency based distribution," *Renew. Energy*, vol. 105, pp. 407–418, May 2017.
- [4] A. Castaings, W. Lhomme, R. Trigui, and A. Bouscayrol, "Practical control schemes of a battery/supercapacitor system for electric vehicle," *IET Electr. Syst. Transp.*, vol. 6, no. 1, pp. 20–26, Mar. 2016.
- [5] G. L. Lopez, R. Schacht Rodriguez, V. M. Alvarado, J. F. Gomez-Aguilar, J. E. Mota, and C. Sandoval, "Hybrid PEMFC-supercapacitor system: Modeling and energy management in energetic macroscopic representation," *Appl. Energy*, vol. 205, pp. 1478–1494, Nov. 2017.
- [6] Z. Ali, Y. Terriche, S. Z. Abbas, M. A. Hassan, M. Sadiq, C.-L. Su, and J. M. Guerrero, "Fault management in DC microgrids: A review of challenges, countermeasures, and future research trends," *IEEE Access*, vol. 9, pp. 128032–128054, 2021.
- [7] C. Yin, H. Wu, F. Locment, and M. Sechilariu, "Energy management of DC microgrid based on photovoltaic combined with diesel generator and supercapacitor," *Energy Convers. Manage.*, vol. 132, no. 15, pp. 14–27, Jan. 2017.
- [8] R. Sebastián, "Application of a battery energy storage for frequency regulation and peak shaving in a wind diesel power system," *IET Gener., Transmiss. Distrib.*, vol. 10, no. 3, pp. 764–770, 2016.
- [9] H. Mahmood, D. Michaelson, and J. Jiang, "A power management strategy for PV/battery hybrid systems in islanded microgrids," *IEEE J. Emerg. Sel. Topics Power Electron.*, vol. 2, no. 4, pp. 870–882, Dec. 2014.
- [10] A. Ahadi, S.-K. Kang, and J.-H. Lee, "A novel approach for optimal combinations of wind, PV, and energy storage system in diesel-free isolated communities," *Appl. Energy*, vol. 170, pp. 101–115, May 2016.
- [11] Z. Cabrane, M. Ouassaid, and M. Maaroufi, "Battery and supercapacitor for photovoltaic energy storage: A fuzzy logic management," *IET Renew. Power Gener.*, vol. 11, no. 8, pp. 1157–1165, 2017.
- [12] K. Venkatraman, B. Dastagiri Reddy, M. P. Selvan, S. Moorthi, N. Kumaresan, and N. A. Gounden, "Online condition monitoring and power management system for standalone micro-grid using FPGAs," *IET Gener., Transmiss. Distrib.*, vol. 10, no. 15, pp. 3875–3884, Nov. 2016.
- [13] K. M. Bhargavi, N. S. Jayalakshmi, D. N. Gaonkar, A. Shrivastava, and V. K. Jadoun, "A comprehensive review on control techniques for power management of isolated DC microgrid system operation," *IEEE Access*, vol. 9, pp. 32196–32228, 2021.
- [14] M. Mehdi, C.-H. Kim, and M. Saad, "Robust centralized control for DC islanded microgrid considering communication network delay," *IEEE Access*, vol. 8, pp. 77765–77778, 2020.
- [15] D. Pavković, M. Lobjrović, M. Hrgetić, and A. Komljenović, "A design of cascade control system and adaptive load compensator for battery/ultracapacitor hybrid energy storage-based direct current microgrid," *Energy Convers. Manage.*, vol. 114, pp. 154–167, Apr. 2016.
- [16] Y. Li, Z. Xu, L. Xiong, G. Song, J. Zhang, D. Qi, and H. Yang, "A cascading power sharing control for microgrid embedded with wind and solar generation," *Renew. Energy*, vol. 132, pp. 846–860, Mar. 2019.
- [17] M. K. Senapati, C. Pradhan, S. R. Samantaray, and P. K. Nayak, "Improved power management control strategy for renewable energy-based DC micro-grid with energy storage integration," *IET Gener., Transmiss. Distrib.*, vol. 13, no. 6, pp. 838–849, Mar. 2019.
- [18] S. Kewat, B. Singh, and I. Hussain, "Power management in PV-battery-hydro based standalone microgrid," *IET Renew. Power Gener.*, vol. 12, no. 4, pp. 391–398, Mar. 2018.
- [19] M. Dong, L. Li, Y. Nie, D. Song, and J. Yang, "Stability analysis of a novel distributed secondary control considering communication delay in DC microgrids," *IEEE Trans. Smart Grid*, vol. 10, no. 6, pp. 6690–6700, Nov. 2019.
- [20] M. Shi, X. Chen, J. Zhou, Y. Chen, J. Wen, and H. He, "Advanced secondary voltage recovery control for multiple HESSs in a droop-controlled DC microgrid," *IEEE Trans. Smart Grid*, vol. 10, no. 4, pp. 3828–3839, Jul. 2019.
- [21] B. Wang, U. Manandhar, X. Zhang, H. B. Gooi, and A. Ukil, "Deadbeat control for hybrid energy storage systems in DC microgrids," *IEEE Trans. Sustain. Energy*, vol. 10, no. 4, pp. 1867–1877, Oct. 2019.
- [22] Z. Liu, Y. Luo, R. Zhuo, and X. Jin, "Distributed reinforcement learning to coordinate current sharing and voltage restoration for islanded DC microgrid," *J. Modern Power Syst. Clean Energy*, vol. 6, no. 2, pp. 364–374, Mar. 2018.
- [23] F. Barati, D. Li, and R. A. Dougal, "Voltage regulation in medium voltage DC systems," in *Proc. IEEE Electr. Ship Technol. Symp. (ESTS)*, Apr. 2013, pp. 372–378.
- [24] F. Barati and B. Ahmadi, "Current sharing in non-coupled interleaved bi-directional boost converters for supercapacitor applications," in *Proc. IEEE 6th Int. Symp. Power Electron. Distrib. Gener. Syst. (PEDG)*, Jun. 2015, pp. 1–5.

- [25] B. Ahmadi, F. Barati, and C. Karimi, "A variable current-limit control scheme for a bi-directional converter used in ultracapacitor applications," *Electr. Power Compon. Syst.*, vol. 46, no. 3, pp. 278–289, Feb. 2018.
- [26] N. Mohan, T. M. Undeland, and W. P. Robbins, *Power Electronics: Converters, Applications, and Design*, 3rd ed. Hoboken, NJ, USA: Wiley, 2003.
- [27] J. Serrano-Delgado, P. Mattavelli, S. Cobreces, H. Abedini, M. Rizo, S. Buso, and E. J. Bueno, "Output capacitance minimization for converters in DC microgrids via multi-objective tuning of droop-based controllers," *IEEE Access*, vol. 8, pp. 222700–222710, 2020.



**BEHZAD AHMADI** received the B.Sc. degree in solid state physics from the University of Tehran, in 2002, and the B.Eng., M.Eng., and Ph.D. degrees in electrical and electronics engineering from Institut National Polytechnique de Grenoble, France, in 2010. He is currently the Lead Electronics Designer working on the design of power HIL systems and high-power converters with D&V Electronics, ON, Canada.



**FARHAD BARATI** received the Ph.D. degree in electrical power engineering from the Sharif University of Technology, Tehran, Iran, in collaboration with the University of Cambridge, Cambridge, U.K., in 2010. He is currently an Assistant Professor with the Department of Energy, Materials and Energy Research Center, Karaj, Iran. His research interests include power electronics converters and their control for renewable sources and energy storages. He received the Postdoctoral Fellowship from the University of South Carolina, Columbia, USA, in 2012.



**OZAN KEYSAN** received the M.Sc. degree from Middle-East Technical University (METU), Ankara, Turkey, in 2008, and the Ph.D. degree from the University of Edinburgh, Edinburgh, U.K., in 2014. He is currently an Associate Professor with the Department of Electrical and Electronics Engineering, METU. His current research interests include renewable energy, design and optimization of electrical machines, smart grids, superconducting machines, and permanent-magnet machines.

• • •